NASA
Technical
Paper
2242

December 1983

A Simple Model of Space Radiation Damage in GaAs Solar Cells

John W. Wilson,
John J. Stith,
and L. V. Stock

NASA

25th Anniversary
1958-1983

NASA
Technical
Paper
2242

1983

A Simple Model of Space Radiation Damage in GaAs Solar Cells

John W. Wilson
Langley Research Center
Hampton, Virginia

John J. Stith
Virginia State University
Petersburg, Virginia

L. V. Stock
Old Dominion University
Norfolk, Virginia

NASA
National Aeronautics
and Space Administration

**Scientific and Technical
Information Branch**

1983

CONTENTS

SUMMARY

A simple model is derived for the radiation damage of shallow-junction gallium arsenide (GaAs) solar cells. Reasonable agreement is found between the model and specific experimental studies of radiation effects with electron and proton beams. In particular, the extreme sensitivity of the cell to protons stopping near the cell junction is predicted by the model. The 1-MeV electron equivalent-fluence ratio is dependent on proton energy and fluence level for monoenergetic proton beams. Angular factors are quite important in establishing the cell sensitivity to incident particle types and energies. A fluence of isotropic-incidence 1-MeV electrons (assuming infinite backing) is equivalent to four times the fluence of normal-incidence 1-MeV electrons. Spectral factors common to the space radiations are considered, and cover-glass thickness required to minimize the initial damage for a typical cell configuration is calculated. Rough equivalence between the geosynchronous environment and an equivalent 1-MeV electron fluence (normal incidence) is established.

INTRODUCTION

Gallium arsenide (GaAs) solar cells have received considerable attention because of their potential usefulness in high-power space-energy systems as well as special space-probe applications where high operating temperature is a limiting factor for silicon solar cells (ref. 1). However, space radiation damage to the GaAs cell may be a limiting factor in Earth orbit above 2000 km and on interplanetary missions unless sufficient shielding is provided to keep damage levels within acceptable limits. Consequently, radiation damage studies have been made (refs. 2 to 10) on the effects of proton and electron irradiation, including defect characterization and annealing. Since damage effects are not generally additive, the combined effects of electron and proton exposure, as well as angular and spectral factors, are not known from the available experimental data base (refs. 2, 5, and 6). To determine design parameters for a specific space environment, extensive laboratory testing or a model of the effects of the specific radiation components on the cell performance is required. Within the context of a detailed model, the question of additivity of specific radiation components can be adequately understood, and the cell performance can be evaluated under appropriate space environmental conditions.

Earlier models for electron radiation damage assumed the defects to be produced uniformly throughout the cell volume and modeled the cell performance in terms of cell-averaged diffusion lengths of the minority carriers (refs. 2 to 4). However, for low-energy protons, defects are not produced uniformly throughout the cell volume. Thus, there is a specific dependence of cell efficiency on proton energy. Consequently, the present report treats the geometric distribution of the displacement damage in detail, and cell performance is evaluated in terms of the cell-averaged minority-carrier recombination probability in diffusion to the cell junction. The average of the minority recombination probability over the cell active region weighted according to the solar-averaged photoabsorption rate is used to estimate the decrement in the short-circuit current.

PROTON DEFECT FORMATION

Atomic displacements caused by proton impact with atomic nuclei result in crystal defects as illustrated in figure 1. The formation rate of these defects is related to Rutherford's cross section (ref. 11):

$$\sigma_D(E) = \frac{4\pi a_o^2 E_R^2 Z_2^2}{M_2 E}\left(\frac{1}{T_D} - \frac{1}{T_m}\right) \tag{1}$$

where a_o is Bohr's radius, E_R is Rydberg's constant, Z_2 is the atomic number of the struck nucleus, M_2 is the corresponding nuclear mass number, E is the proton kinetic energy, T_D is the energy required to displace the nucleus from its lattice site, and T_m is the maximum energy transfer in the collision. T_m is given by

$$T_m = \frac{4M_2}{(1 + M_2)^2} E \tag{2}$$

The displacement cross section and average energy transfer for protons in GaAs with $Z_2 \approx 32$ and $M_2 \approx 72.5$ are shown in figures 2 and 3. The threshold for displacement requires that $T_M > T_D$. The fact that $T_D \approx 9.5$ eV (ref. 12) insures that only close collisions result in displacement, so that screening corrections to the Rutherford formula are unimportant (ref. 11). If the atomic recoil energy is sufficiently large ($T >> T_D$), additional displacements can be produced by the recoiling nucleus before coming to rest at an interstitial site. The average number of recoil displacements produced by one initiating proton collision event is given as a function of the maximum energy transfer by

$$\bar{\nu}_D(E) = \begin{cases} 1 + \dfrac{T_m}{2(T_m - T_D)} \log\left(\dfrac{T_m}{T_D}\right) & (T_m > 2T_D) \\ 1.0 & (2T_D \geq T_m > T_D) \end{cases} \tag{3}$$

with the assumption that half the recoil energy produces further displacements and the other half is dissipated in other processes (ref. 11). These quantities allow the calculation of the number of displacements produced per unit distance traveled by a proton of fixed energy.

In passing through a crystal, most of the energy of a proton is transferred to orbital electrons (ref. 13). The path length traveled in coming to rest is found by fitting the data of Andersen and Ziegler (ref. 13) as

$$P(E) = 0.077E^{0.5} + 1.125 \times 10^{-4} E^{1.64} \tag{4}$$

where E is in keV and $P(E)$ is in μm. As derived from the slowing-down theory, a unique value of kinetic energy can be associated with each position along the trajectory of a proton. The proton energy as a function of the distance p yet to be traveled before coming to rest is given by

$$E = (209.6p^{2.08})/(1 + 1.055p^{1.43}) \tag{5}$$

as determined by integrating the stopping-power data of Andersen and Ziegler (ref. 13). In the process of coming to rest, the proton undergoes multiple scatterings from atomic nuclei, of which a few result in displacements. This process alters ever so slightly the direction of motion of the proton. The depth of penetration $R(E)$ and path length $P(E)$ are approximately related (ref. 13) by

$$P(E)^{-1}R(E) = [1 - \exp(-0.084E^{0.55})] \tag{6}$$

This ratio is related to the average deviation in the direction of motion and is most important at low energies. The average depth of penetration and initial energy as related through equations (4) and (6) can be approximated by

$$R(E) = 0.0062E + 2.92 \times 10^{-5}E^{1.77} \tag{7}$$

There is no unique energy associated with a given depth of penetration due to multiple scattering. However, the average energy of protons which penetrate and stop at a depth x is

$$E = 593x^{1.5}/(x + 3.71x^{0.5}) \tag{8}$$

The preceding quantities were used to determine the displacement density within a GaAs crystal.

A proton of energy E_o incident on the face of the crystal travels a distance

$$P_o = P(E_o) \tag{9}$$

before coming to rest. After traveling a distance p the energy will be reduced to

$$E = [209.6(P_o - p)^{2.08}]/[1 + 1.055(P_o - p)^{1.43}] \tag{10}$$

At this position p, the displacement mean free path is

$$\ell_D(E) = \frac{1}{n}\sigma_D(E) \tag{11}$$

where n is the density of scattering centers in the crystal ($4.42 \times 10^{10}/\mu m^3$), and $\sigma_D(E)$ is the displacement cross section averaged for GaAs ($M_2 = 72.5$ and $Z_2 = 32$). The average number of displacements per unit path length is

$$\xi_D(E) = \bar{\nu}_D(E)/\ell_D(E) \tag{12}$$

The use of equations (10) and (12) allows appropriate partitioning of the proton energy into electronic excitation and displacements everywhere along its path.

The number of displacements along the proton path is related to the displacement damage in the crystal. For normal incident protons of energy E_o on the face of a crystal, the number of displacements along its path is given by equations (10) and (12). However, by the time its energy is reduced to E, it has penetrated to an average depth x given by

$$x = R(E_o) - R(E) \tag{13}$$

The path length and penetration depth are related to the average direction cosine (ref. 14) and are approximated here by solving the equation $\bar{\mu}(E) = dP(E)/dR(E)$ using equations (4) and (6). In terms of $\bar{\mu}(E)$, the average number of displacements per unit depth is

$$\frac{dD(E)}{dx} = \bar{\mu}(E)\ \xi_D(E) \tag{14}$$

where x is found from equation (13). The effects of multiple scattering are demonstrated in figure 4. The results of equation (14) for the average proton path due to multiple scattering (solid line) are compared with calculations neglecting multiple scattering (dashed line) according to equation (12). The difference between the two curves is a measure of the fluctuations caused by multiple scattering.

The total number of displacements formed along the path of a proton with initial energy E_o is

$$D(E_o) = \int_0^{E_o} \xi_D(E)\ \frac{dP(E)}{dE}\ dE \tag{15}$$

The numerical evaluation of equation (15) as shown in figure 5 is approximated by

$$D(E_o) = \begin{cases} 0 & (E_o \leq 0.64) \\ 12.4 + 350.4\ (1 - 0.8236\ E_o^{0.016})\ \log_{10}(E_o) & (0.64 \leq E_o \leq 20) \\ 47.83 + 20.48\ (1 + 3.246 \times 10^{-3}\ E_o^{0.721})\ \log_{10}(E_o) & (20 \leq E_o) \end{cases} \tag{16}$$

where the effective threshold displacement energy for the proton is 0.64 keV. Equation (15) was also evaluated using the displacement theory of Lindhard, Scharff, and Schiott (LSS) as discussed in reference 15. The numerical values of the LSS theory and the present results are in good agreement. (See ref. 9.)

ELECTRON DEFECT FORMATION

One of the significant differences between proton and electron interaction is that relativistic effects must be included in the electron interaction. The Mott-McKinley-Feshbach (refs. 16 and 17) relativistic electron scattering cross section leads to the expression

$$d\sigma = \pi r_c^2 Z_2^2 \left(\frac{1 - \beta^2}{\beta^4}\right)\left(\frac{T_m}{T^2} - \frac{\beta^2}{T} + \pi\alpha\beta T_m T^{-3} - \frac{\pi\alpha\beta}{T}\right) dT \tag{17}$$

where T is the energy transferred in the collision, r_c is the classical electron radius, Z_2 is the atomic number of the target atom, β is the ratio of the electron velocity to the speed of light, and α equals $Z_2/137$. Integration yields the displacement cross section shown in figure 2 and given by

$$\sigma_D(E) = \pi Z_2^2 r_c^2 \left(\frac{1 - \beta^2}{\beta^4}\right)\left[\frac{T_m}{T_D} - 1 - \beta^2 \log\left(\frac{T_m}{T_D}\right) + 2\pi\alpha\beta\left(\frac{T_m}{T_D} - 1\right) - \pi\alpha\beta \log\left(\frac{T_m}{T_D}\right)\right] \tag{18}$$

where the maximum energy transfer is

$$T_m = \frac{2E}{M_2 c^2}(E + 2mc^2) \tag{19}$$

and M_2 is the mass of the atom, m is the mass of the electron, T_D is the displacement threshold, and c is the velocity of light. In a collision between an electron of energy E and an atom, the atom acquires an energy in excess of T_D for cross section $\sigma_D(E)$.

A requirement for displacement of a nucleus is that $T > T_D$. The value of T_D used in deriving this model is 9.5 eV (ref. 12). The average energy transfer during a collision is

$$\bar{T}(E) = \frac{1}{\sigma_D(E)} \int_{T_D}^{T_m} T(E) \frac{d\sigma_D(E)}{dT} dT$$

$$= \frac{T_m \log\left(\frac{T_m}{T_D}\right) - \beta^2(T_m - T_D) + 2\pi\alpha\beta(T_m - T_m T_D) - \pi\alpha\beta(T_m - T_D)}{\frac{T_m}{T_D} - 1 - \beta^2 \log\left(\frac{T_m}{T_D}\right) + 2\pi\alpha\beta\left(\frac{T_m}{T_D} - 1\right) - \pi\alpha\beta \log\left(\frac{T_m}{T_D}\right)} \tag{20}$$

Figure 3 illustrates the dependence on electron energy of the average energy transfer between an electron of initial energy E and a gallium or arsenic atom. If the energy transfer $T(E) >> T_D$, additional atomic displacements can be produced by the initial recoiling nucleus before it comes to rest at an interstitial or replacement site. The average number of recoils caused by one electron colliding with an atom is given as a function of the average energy transfer by

$$\bar{\nu}_D(E) = \begin{cases} 1 & (T_D \leq \bar{T}(E) \leq 2T_D) \\ 1 + \frac{\bar{T}(E)}{2T_D} & (\bar{T}(E) > 2T_D) \end{cases} \tag{21}$$

assuming half the recoil energy produces further displacements and assuming the other half is dissipated in other processes.

The displacement mean free path is

$$\ell_D(E) = 1/n\sigma_D(E) \tag{22}$$

where n is the density of scattering centers in the crystal ($4.42 \times 10^{22}/cm^3$) and $\sigma_D(E)$ is the displacement cross-section average for GaAs ($M_2 = 72.5$ and

$Z_2 = 32$). The average number of displacements per unit path length produced by an electron of initial energy E is

$$\xi_D(E) = \bar{\nu}_D(E)/\ell_D(E) = n\,\bar{\nu}_D(E)\,\sigma_D(E)$$

$$= \begin{cases} n\,\sigma_D(E) & (T_D < \bar{T}(E) < 2T_D) \\ n\,\sigma_D(E) + \dfrac{n}{2T_D}\,\sigma_D(E)_D\,\bar{T}(E) & (\bar{T}(E) > 2T_D) \end{cases} \tag{23}$$

The total number of displacements produced along the path of an electron of initial energy E_o is

$$D(E_o) = \int_0^{E_o} \frac{\xi_D(E)}{S(E)}\,dE = n\int_0^{E_o} \frac{\bar{\nu}(E)\,T_D(E)}{S(E)}\,dE \tag{24}$$

where

$$S(E) = \begin{cases} 0.381E^{0.084} & (260 < E < 1000\ \text{keV}) \\ 0.623 + 4.25 \times 10^{-5}E & (1000 \leq E \leq 10\,000\ \text{keV}) \end{cases} \tag{25}$$

is the stopping-power formula (keV/μm) determined from data in reference 18. Numerical evaluation of the displacement integral can be approximated by

$$D(E) = \begin{cases} 0 & (E < 260\ \text{keV}) \\ -3.6 + 3.32 \times 10^{-3}E + 3.58\exp(-1.094 \times 10^{-3}E) & (260 \leq E \leq 10\,000\ \text{keV}) \end{cases} \tag{26}$$

Figure 5 illustrates the dependence of atomic displacements in GaAs on initial electron energy as found from evaluation of equation (24).

In passing through the crystal, the electron is slowed down as it interacts with orbital electrons and atomic nuclei. Using data from reference 18, the range of the electron in GaAs as a function of initial electron energy E is given by

$$R(E) = 0.4027E^{1.16} - 5.95 \times 10^{-5}E^2 \tag{27}$$

where $R(E)$ is in μm and E is in keV. The effects of multiple scattering are neglected in this formula for $R(E)$ because multiple scattering of electrons is relatively unimportant in the thin GaAs cells treated herein.

From the same data used in determining the range formula, a formula for the average energy of an electron that penetrates to a depth R and stops is

$$E = 2.217R^{0.86} + (2.25 \times 10^{-5})R^2 \tag{28}$$

After penetrating to a depth of x within the crystal, the electron energy is given by

$$E_o(x) = 2.217(R_o - x)^{0.86} + 2.25 \times 10^{-5}(R_o - x)^2 \tag{29}$$

The effect of these radiation-induced defects on cell performance is discussed in the section which follows.

MINORITY-CARRIER RECOMBINATION

It is assumed that these radiation-induced displacements within the crystal form recombination centers for the minority carriers of the electron-hole pairs produced by photon absorption. A minority carrier, once formed, undergoes thermal diffusion until it is trapped and recombines or is separated at the junction. The root-mean-square distance traveled in moving to a position a distance L away from the source point is (ref. 19)

$$\bar{r} = \sqrt{6}\, L \tag{30}$$

If σ_r is the recombination cross section and L is the distance along an arbitrary straight line path to the junction, the fractional loss of pairs due to recombination in reaching the junction along a fixed direction is

$$f(\mu) = \begin{cases} \left\{1 - \exp\left[-\int_{x_j}^{x} \sigma_r D_v(x) \sqrt{6}\, \frac{dx}{\mu}\right]\right\} & (x > x_j) \\ \left\{1 - \exp\left[-\int_{x}^{x_j} \sigma_r D_v(x) \sqrt{6}\, \frac{dx}{\mu}\right]\right\} & (x < x_j) \end{cases} \tag{31}$$

where μ is the cosine of the direction to the junction, and $D_v(x)$ is the displacement density. Averaging the fractional loss over all directions toward the junction

$$F(x) = \int_0^1 f(\mu)\, d\mu \tag{32}$$

results in

$$F(x) = 1 - E_2\left[\sqrt{6}\,\sigma_r \left| \int_x^{x_j} D_v(x)\, dx \right|\right] \tag{33}$$

where summations over all spectral and angular components are implied. Note that $E_2(z)$ is the exponential integral of order 2.

The photoabsorption rate density at a depth x within the cell for the solar spectrum is

$$\rho(x) = K\gamma \exp(-\gamma x) \tag{34}$$

where K is the integrated flux in the absorption band, and γ is the photoabsorption coefficient averaged over the solar spectrum ($\gamma \approx 1.4\ \mu m^{-1}$). The rate at which the photocurrent is collected under short-circuit conditions is

$$I_{sc,o} = \int_0^t \eta_c(x)\, \rho(x)\, dx \tag{35}$$

where $\eta_c(x)$ is the normal or pre-irradiated collection efficiency, and t is the depth of the active region. The normal collection efficiency is known in terms of diffusion lengths, lifetimes, and surface recombination rates of the minority carriers; electric fields; and cell dimensions (ref. 20).

To derive a simple expression for the short-circuit current in an irradiated cell, the following simplifying assumptions are made. First, it is assumed that the radiation-induced defects do not greatly alter the internal-cell electric fields. It is further assumed that the radiation defects mainly alter the cell operation through change in the minority-carrier lifetime in the bulk. Surface recombination plays only a secondary role for heteroface cells. (See refs. 2 and 3.) Viewing $\eta_c(x)$ as a probability of current collection of an electron-hole pair produced at x, it is further assumed that the normal collection efficiency and the recombination

probability with radiation defects are statistically independent. This independence, which allows the post-irradiation short-circuit current to be written as

$$I_{sc} = \int_0^t \eta_c(x)[1 - F(x)]\, \rho(x)\, dx \tag{36}$$

for which the fractional remaining current is

$$I_{sc}/I_{sc,o} = 1 - \left[\int_0^t \eta_c(x)\, F(x)\, \rho(x)\, dx \Big/ \int_0^t \eta_c(x)\, \rho(x)\, dx\right] \tag{37}$$

For a well-designed high-collection-efficiency solar cell, $\eta_c(x)$ is nearly spatially independent over the cell active volume, so that further simplification results in

$$I_{sc}/I_{sc,o} \approx 1 - \left[\int_0^t F(x)\, \rho(x)\, dx \Big/ \int_0^t \rho(x)\, dx\right] \tag{38}$$

which is used throughout the remainder of the present work.

EVALUATION OF DEFECT SPATIAL DISTRIBUTION

Central to the calculation of radiation effects as outlined in the preceding section is evaluation of the integral of the defect volume density. This integral is related to a cumulative defect function by

$$D_c(x) = \int_0^x D_v(x')\, dx' \tag{39}$$

This quantity may be evaluated for a fluence $\phi(E_o)$ of normally incident particles of energy E_o. This is accomplished by simply calculating the particle residual energy $E_o(x)$ after penetrating to a depth x and noting that

$$D_c(x) = \{D(E_o) - D[E_o(x)]\}\, \phi(E_o) \tag{40}$$

Since $E_o(x)$ is the residual-energy function for normal incidence, the corresponding result for oblique incidence is

$$D_c(x) = \left\{D(E_o) - D\left[E_o(x/\cos\theta)\right]\right\} \phi(E_o) \tag{41}$$

where θ is the angle of incidence to the normal of the surface. Generalizing for a spectrum of particles and isotropic incidence,

$$D_c(x) = 2\pi \int_0^\infty dE_o \int_0^1 d(\cos\theta)\left\{D(E_o) - D\left[E_o(x/\cos\theta)\right]\right\} \phi(E_o) \tag{42}$$

where $4\pi\phi(E_o)$ is the omnidirectional differential fluence spectrum.

COMPARISON WITH EXPERIMENT

The geometry of the solar cells used in experimental tests (refs. 5 and 6) is shown in figure 6. The changes in the cell current collection efficiency as given by equation (38) were evaluated numerically and are shown in figure 7 for the solar-cell parameters shown in figure 6. Since the protons follow neither the trajectory of the average proton nor the trajectory in which multiple scattering is neglected (fig. 4), improvements were made by including the effects of multiple scattering. These effects were estimated by averaging with equal weight the cell damage for the two functions shown in figure 4, in which some effects of deviations about the average trajectory are included. It is clear that an understanding of the low-energy experimental data requires detailed modeling of multiple scattering effects. The window thickness parameters which varied from cell to cell in experimental tests (refs. 5 and 6), were assumed to be governed by a uniform distribution in the present calculations. The model results averaged over the window thickness are compared with short-circuit current measurements (refs. 5 and 6) of irradiated cells shown in figure 7. The best value of recombination cross section is

$$\sigma_r \approx 6 \times 10^{-14} \text{ cm}^2 \tag{43}$$

which is in fair agreement with the estimated average cross section ($\sigma_r \approx 1.06 \times 10^{-13}$ cm^2) determined from deep-level transient spectroscopy (ref. 7).

The fractional short-circuit current remaining after 1 MeV of electron irradiation is shown as a function of electron fluence in figure 8. The recombination cross section was

$$\sigma_r \approx 4 \times 10^{-14} \text{ cm}^2 \tag{44}$$

and calculations were made for two junction depths, namely 0.5 μm and 0.8 μm. Also shown in figure 8 are corresponding experimental data of references 3 and 21. The reasonable consistency of the theory for vastly different particle types is gratifying.

EQUIVALENT ELECTRON-FLUENCE CONCEPT

It is customary in protection from mixed-radiation environments to develop concepts under which effects of radiations of different quality may be combined to ascertain the total effect on device performance. From an electronic-device standpoint, the equivalent-electron fluence is usually employed as the combinational rule. The equivalent electron fluence is defined as that fluence of electrons of fixed energy (usually 1 MeV) which produces the same effect on the device performance as a particle fluence of a particular type, energy, and fluence level. The fluence of electrons ϕ_e equivalent to a fluence of protons $\phi_p(E_p)$ of energy E_p is given by

$$R_p\left[\phi_p(E_p)\right] = R_e(\phi_e) \tag{45}$$

where R_p and R_e are the device response functions for proton and electron damage (ref. 22). If equation (45) is satisfied, the equivalent-fluence ratio may be defined as

$$r_f(E_p) = \phi_e/\phi_p(E_p) \tag{46}$$

and the main usefulness of the concept requires that $r_f(E_p)$ not depend on the magnitude of $\phi_p(E_p)$. The equivalence for solar cells is usually related through the minority-carrier diffusion length for which the equivalent-fluence ratio is expressed as the ratio of the damage coefficients (refs. 10 and 22). The combined effects of electron and proton exposure are then

$$R_{tot}\left[\phi_p(E_p),\phi_e\right] = R_e\left[\phi_e + r_f(E_p)\ \phi_p(E_p)\right] \tag{47}$$

where ϕ_e and $\phi_p(E_p)$ are the mixed environmental components. The strong energy dependence of the response to protons arising from spatial nonuniformity in cell damage brings into question the usefulness of the concept of equivalent electron fluence (refs. 10 and 22).

The remaining short-circuit current for 0.4-μm window cells and 0.5-μm junction cells as a function of proton energy and fluence is shown in figure 9. The equivalent-fluence ratio was calculated using equations (45) and (46) for 1-MeV electron-fluence levels $\phi_e = 1.7 \times 10^{15}$ electrons/cm^2, 6.8×10^{15} electrons/cm^2, and 2.3×10^{16} electrons/cm^2 at $I_{sc}/I_{sc,o} = 0.8$, 0.5, and 0.2 (as seen in fig. 8 for the 0.5-μm junction cell). The resulting values of $r_f(E_p)$ are shown in figure 10 for each of the three fluence levels. For the equivalent-fluence concept to be useful, the three curves must coincide at all proton energies as they do above 500 keV. However, in the proton energy range 50 to 500 keV, where the cell is extremely sensitive, the usefulness of equivalent electron fluence is generally limited by the strong dependence of the equivalent-fluence ratio on the damage level. This has

important consequences in terms of radiation testing, since the mixed environment generally must be simulated to insure a valid test unless the bivariate equivalent-fluence ratio is adequately known. On the other hand, for a given (fixed) environment, test procedures could be established through the use of the present model, for a given cell type. Thus, an "equivalent" electron fluence could be established in the restricted sense of fixed environmental components.

ANGULAR ISOTROPY EFFECTS

The radiation in space can, for most practical purposes, be considered isotropic, and most radiation models present the data as the omnidirectional fluence. Such angular factors generally have great importance in radiation protection problems (ref. 10), and such effects within the context of this simple model are evaluated here. The relationship between the defect density distribution within the cell and cell performance having been established, the defect density is now evaluated for isotropic-incidence monoenergetic protons by replacing $\phi(E_o)$ in equation (42) with a δ-function. Results are shown in figure 11. Clearly, angular isotropy effects show no major differences in cell sensitivity at all energies and fluence levels, although a general increase in radiation resistance at the lowest fluence levels is apparent. However, at the high fluence levels, the sensitivity is increased in the 200-keV to 1-MeV region. At higher energies ($E >> 1$ MeV), angular factors are relatively less important because of the high penetrating power of the protons.

In general, the angular factors are helpful if fluence levels are sufficiently low that the reduced penetration of low-energy protons at oblique angles of incidence serves to provide the cell with added protection. At high fluence levels and fixed energy, the minority-carrier recombination rates near the end of the proton trajectories tend to saturate for normal incidence, whereas isotropic incidence tends to distribute these defects more uniformly over the cell. This uniform distribution increases their effectiveness for cell damage, which in turn accounts for the increased cell sensitivity for $E > 200$ keV (as shown in fig. 11 for $\phi_p = 10^{12}$ protons/cm^2). The spectral characteristics for performance evaluation in space applications must still be considered in the protection against space radiation.

Solar-cell performance is likewise evaluated for isotropic-incidence 1-MeV electrons. The results are shown in figure 12 as a function of omnidirectional fluence level (0.5-μm junction depth and infinite backing is assumed). Comparison of figure 12 with figure 8 for normal incidence shows that an isotropically incident electron is equivalent to four normal-incidence electrons. Clearly, isotropic incidence is a most important factor for space radiation testing.

EFFECTS OF SPACE RADIATION ENVIRONMENT

Space missions to the fringes of the geomagnetic field and interplanetary missions experience the yearly solar-particle fluence during highly solar-active years (ref. 23) on the order of

$$\phi_p(E_p) \approx \frac{5 \times 10^{14}}{E_p} \tag{48}$$

where E_p is in keV and ϕ_p is in protons/cm^2. The remaining short-circuit current calculated from equations (38) and (48) as a function of cover-glass thickness is shown in figure 13. It is clear that an unshielded cell would not survive a major solar event and requires a cover glass of about 25 μm to insure performance levels to within 90 percent of their initial value.

The protons (ref. 24) trapped at geosynchronous altitude (L = 6.6 Earth radii) are well approximated by

$$\phi_p(E_p) = 2.5 \times 10^{14} \exp\left[-1.27 - 0.0072E_p + \frac{230}{E_p}\right] \tag{49}$$

where ϕ_p is in protons/cm^2-yr. The corresponding yearly electron fluence (ref. 25) is

$$\phi_e(E_e) = 4.5 \times 10^{14} \exp(-2.832 \times 10^{-3}E_e) \tag{50}$$

in electrons/cm^2-yr. The short-circuit current ratio is calculated for equivalent 1-, 5-, and 10-yr missions in the trapped environment with results shown in figure 14 as a function of cover-glass thickness. Equations (48) to (50) are integrated flux and must be differentiated for use in equation (42). A 15-μm glass cover is required to stop the geosynchronous trapped protons. Cover-glass thickness beyond 15 μm is ineffective for protection against the electron environment. The effects of the geosynchronous trapped environment are combined with a single large solar event in figure 15 for 1-, 5-, and 10-yr missions. Little improvement in cell protection is obtained by having a cover-glass thickness in excess of about 30 μm.

CONCLUDING REMARKS

A simple model for the short-circuit current reduction is derived and shown to correlate well (to within 0.15 of the experimental short-circuit current ratios) with energy-dependent proton and 1-MeV electron damage experiments. The model utilizes the defect density distribution within the cell, which is intimately related to the exposure environment. By using the model, the short-circuit current reduction for a broad range of environmental conditions may be estimated by calculating the corresponding defect density distribution. The model serves to bridge the gap between limited laboratory testing and predicted response in the space environment.

The protection against the trapped geosynchronous environment provided by a cover glass is of little use beyond ≈15 μm, because the highly penetrating electrons cannot be stopped except by very thick glass. If a large solar proton event occurs, a total glass shield of ≈30 μm must be provided.

Langley Research Center
National Aeronautics and Space Administration
Hampton, VA 23665
November 16, 1983

REFERENCES

1. Solar Power Satellite Concept Evaluation, Activities Report - July 1976 to June 1977. Volume I - Summary. JSC-12973, NASA Johnson Space Center, July 1977. (Available as NASA TM-74820.)

2. Walker, Gilbert H.; and Conway, Edmund J.: Short Circuit Current Changes in Electron Irradiated GaAlAs/GaAs Solar Cells. Thirteenth IEEE Photovoltaic Specialists Conference - 1978, pp. 575-579.

3. Walker, Gilbert H.; and Conway, Edmund J.: Recovery of Shallow Junction GaAs Solar Cells Damaged by Electron Irradiation. J. Electrochem. Soc., vol. 125, no. 10, Oct. 1978, pp. 1726-1727.

4. Heinbockel, J. H.; Conway, E. J.; and Walker, G. H.: Simultaneous Radiation Damage and Annealing of GaAs Solar Cells. Fourteenth IEEE Photovoltaic Specialists Conference - 1980, pp. 1085-1089.

5. Loo, R.; Knechtli, R. C.; and Kamath, G. S.: Enhanced Annealing of GaAs Solar Cell Radiation Damage. Fifteenth IEEE Photovoltaic Specialists Conference - 1981, pp. 33-37.

6. Kamath, G. S: GaAs Solar Cells for Space Application. Proceedings of the 16th Intersociety Energy Conversion Engineering Conference. Volume I - Technologies for the Transition. American Soc. Mech. Eng., 1981, pp. 416-421.

7. Li, S. S.; Chiu, T. T.; Schoenfeld, D. W.; and Loo, R. Y.: Defect Characterization and Thermal Annealing Study of 200 KeV Proton Irradiated n-GaAs LPE Layers. Defects and Radiation Effects in Semiconductors, 1980, R. R. Hasiguti, ed., Inst. Phys., c.1981, pp. 335-340.

8. Conway, E. J.; Walker, G. H.; and Heinbockel, J. H.: A Thermochemical Model of Radiation Damage and Annealing Applied to GaAs Solar Cells. Fifteenth IEEE Photovoltaic Specialists Conference - 1981, pp. 38-44.

9. Wilson, John W.; Walker, Gilbert H.; Outlaw, R. A.; and Stock, L. V.: A Model for Proton-Irradiated GaAs Solar Cells. Sixteenth IEEE Photovoltaic Specialists Conference - 1982, pp. 1441-1442.

10. Wilson, John W.; Stith, John J.; and Walker, Gilbert H.: On the Validity of Equivalent Electron Fluence for GaAs Solar Cells. Sixteenth IEEE Photovoltaic Specialists Conference - 1982, pp. 1439-1440.

11. Dienes, G. J.; and Vineyard, G. H.: Radiation Effects in Solids. Interscience Pub., Inc., 1957, pp. 12-32.

12. Bauerlein, R.: Messung der Energie zur Verlagerung eines Gitteratoms durch Elektronenstoss in A^{III} B^{V}-Verbindugen. Z. Phys., vol. 176, no. 4, 1963, pp. 498-509.

13. Andersen, H. H.; and Ziegler, J. F.: Hydrogen Stopping Powers and Ranges in All Elements. Pergamon Press, Inc., c.1977.

14. Janni, Joseph F.: Calculations of Energy Loss, Range, Pathlength, Straggling, Multiple Scattering, and the Probability of Inelastic Nuclear Collisions for 0.1- to 1000-Mev Protons. AFWL-TR-65-150, U.S. Air Force, Sept. 1966. (Available from DTIC as AD 643 837.)

15. Peterson, N. L.; and Harkness, S. D., eds.: Radiation Damage in Metals. American Soc. for Metals, c.1976.

16. Vook, Frederick L., ed.: Radiation Effects in Semiconductors. Plenum Press, 1968.

17. McKinley, William A., Jr.; and Feshbach, Herman: The Coulomb Scattering of Relativistic Electrons by Nuclei. Phys. Rev., second ser., vol. 74, no. 12, Dec. 15, 1948, pp. 1759-1763.

18. Pages, Lucien; Bertel, Evelyne; Joffre, Henri; and Sklavenitis, Laodamas: Energy Loss, Range, and Bremsstrahlung Yield for 10-keV to 100-MeV Electrons in Various Elements and Chemical Compounds. At. Data, vol. 4, no. 1, Mar. 1972, pp. 1-127.

19. Liverhant, S. E.: Nuclear Reactor Physics. John Wiley & Sons, Inc., c.1960, p. 252.

20. Hovel, Harold J.: Semiconductors and Semimetals. Volume 11 - Solar Cells. Academic Press, Inc., 1975, pp. 18-22.

21. Loo, R.; Goldhammer, L.; Anspaugh, B.; Knechtli, R. C.; and Kamath, G. S.: Electron and Proton Degradation in (AlGa)As-GaAs Solar Cells. Thirteenth IEEE Photovoltaic Specialists Conference - 1978, pp. 562-570.

22. Tada, H. Y.; and Carter, J. R., Jr.: Solar Cell Radiation Handbook. JPL Publ. 77-56 (Contract NAS7-100), California Inst. Technol., Nov. 1977. (Available as NASA CR-155554.)

23. Foelsche, T.: Specific Solar Flare Events and Associated Radiation Doses. Space Radiation Effects, ASTM Special Tech. Publ. No. 363, 1963, pp. 1-13.

24. Sawyer, Donald M.; and Vette, James I.: AP-8 Trapped Proton Environment for Solar Maximum and Solar Minimum. NSSDC/WDC-A-R&S 76-06, NASA Goddard Space Flight Center, Dec. 1976. (Available as NASA TM X-72605.)

25. Singley, G. Wayne; and Vette, James I.: The AE-4 Model of the Outer Radiation Zone Electron Environment. NSSDC 72-06, NASA Goddard Space Flight Center, 1972.

SYMBOLS

a_o	Bohr's radius, 5.29×10^{-5} μm
c	velocity of light, cm/sec
D(E)	total number of displacements per particle of energy E
$D_c(x)$	real density of defects, μm^{-2}
$D_v(x)$	number of displacements per unit volume, μm^{-3}
E	particle energy, keV
E_o	initial particle energy, keV
$E_2(z)$	exponential integral of order 2 with argument z
E_R	Rydberg's constant, 13.6 eV
$E_o(x)$	residual energy of particle of initial energy of E_o after penetrating to depth x, keV
$f(\mu)$	efficiency function for diffusion to junction along direction defined by μ
F(x)	efficiency function for diffusion from depth x to junction
I_{sc}	short-circuit current, amps
K	total photon flux in photocell absorption band
$\ell_D(E)$	displacement mean free path for particle of energy E, μm
L	minority-carrier diffusion length, μm
m	mass of electron
M_2	average mass of gallium and arsenic nucleus
n	nuclear density in GaAs crystal, μm^{-3}
p	distance traveled along proton path, μm
P(E)	path length of proton of energy E, μm
P_o	initial particle penetration depth, μm
$\bar{r}$	minority-carrier root-mean-square distance traveled before recombination, μm
r_c	classical electron radius, m
$r_f(E_p)$	equivalent-fluence ratio

$R(E)$ average projected range of a proton of energy E, μm

R_o penetration depth of a particle of initial energy E_o, μm

$R_e(\phi_e)$ solar-cell response to electron fluence ϕ_e

$R_p(\phi_p)$ solar-cell response to proton fluence ϕ_p

$R_{tot}(\phi_p, \phi_e)$ solar-cell response to combined fluences of protons ϕ_p and electrons ϕ_e

t depth of active region, μm

$T(E)$ energy transferred to struck nucleus, eV

T_D displacement damage threshold, eV

T_m maximum energy transferred to struck nucleus, eV

x penetration depth into solar cell, μm

x_j junction depth, μm

Z_2 average charge number of GaAs nucleus

α fine structure constant, $Z_2/137$

β ratio of particle velocity to velocity of light

γ photon absorption path length, μm

$\eta_c(x)$ cell-charge collection efficiency for electron-hole pair produced at x

θ angle of incidence of particle, deg

μ cosine of direction of diffusion in reaching junction

$\bar{\mu}(E)$ average direction cosine of scattered proton of energy E

$\bar{\nu}_D(E)$ average number of displacements formed by one particle-scattering event

$\xi_D(E)$ number of displacements per unit path length for particle of energy E, μm^{-1}

$\rho(x)$ cell collection efficiency for a normal unirradiated cell, μm^{-3}

σ nuclear scattering cross section, μm^2

$\sigma_D(E)$ displacement cross section for particle of energy E, μm^2

σ_r recombination cross section, μm^2

$\phi(E_o)$ particle fluence at energy E_o, cm^{-2}

Subscripts:

e electron

p proton

A bar over a symbol denotes an average. Prime denotes variable of integration.

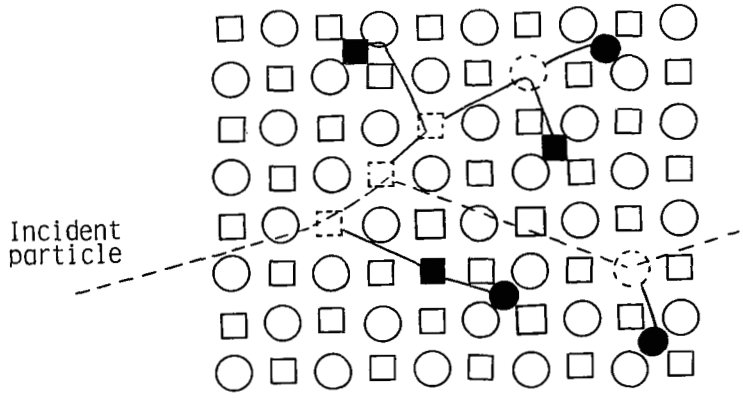

Figure 1.- Defect formation by particulate radiation in a binary crystal. Defects shown are replacements, vacancies, and interstitials.

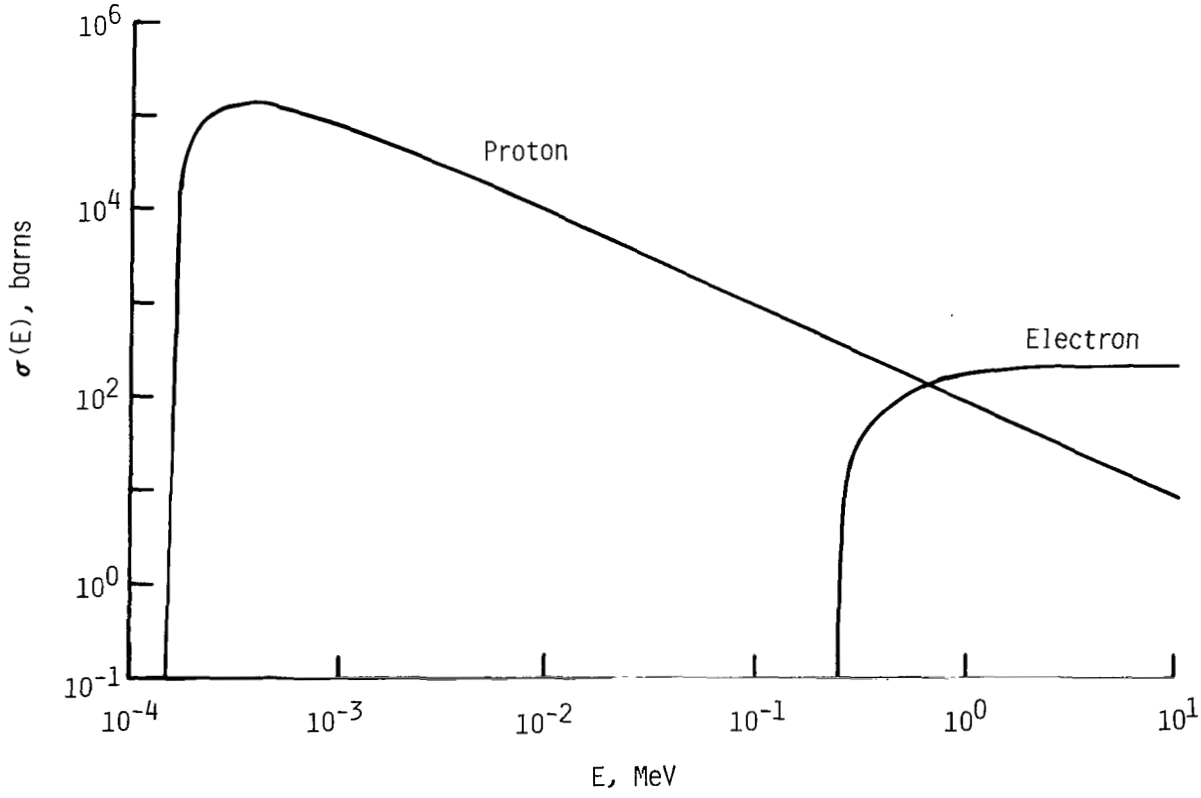

Figure 2.- Displacement cross section for energetic protons and electrons. 1 barn = 1×10^{-28} cm^2.

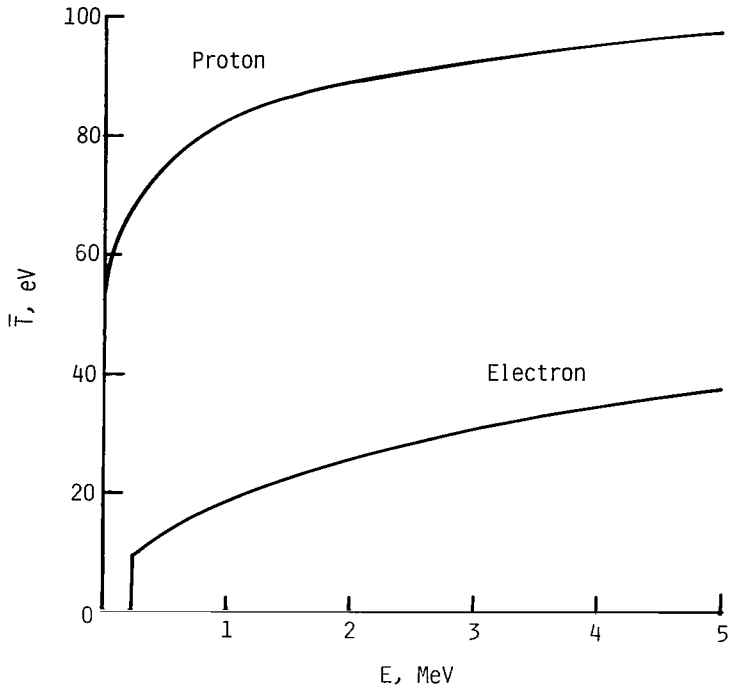

Figure 3.- Average energy transferred to recoiling nucleus.

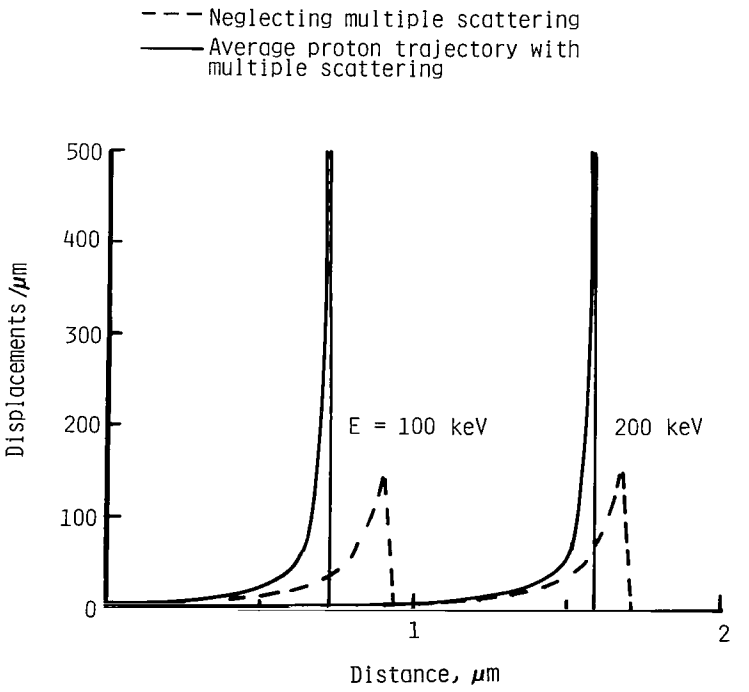

Figure 4.- Displacement density for a single proton path.

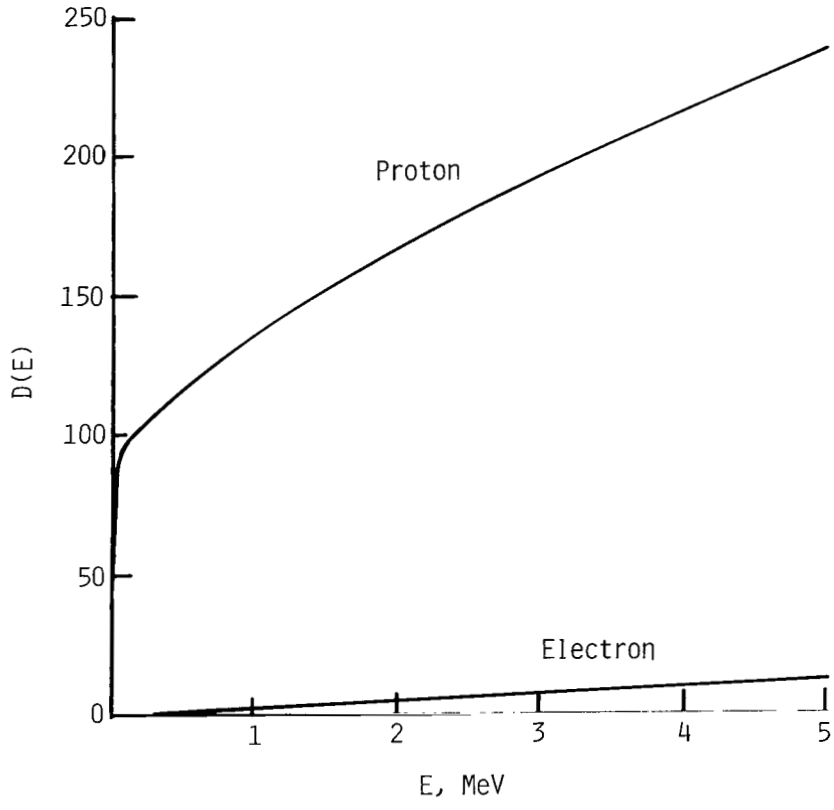

Figure 5.- Total number of defects formed in bringing a particle to rest in GaAs crystal.

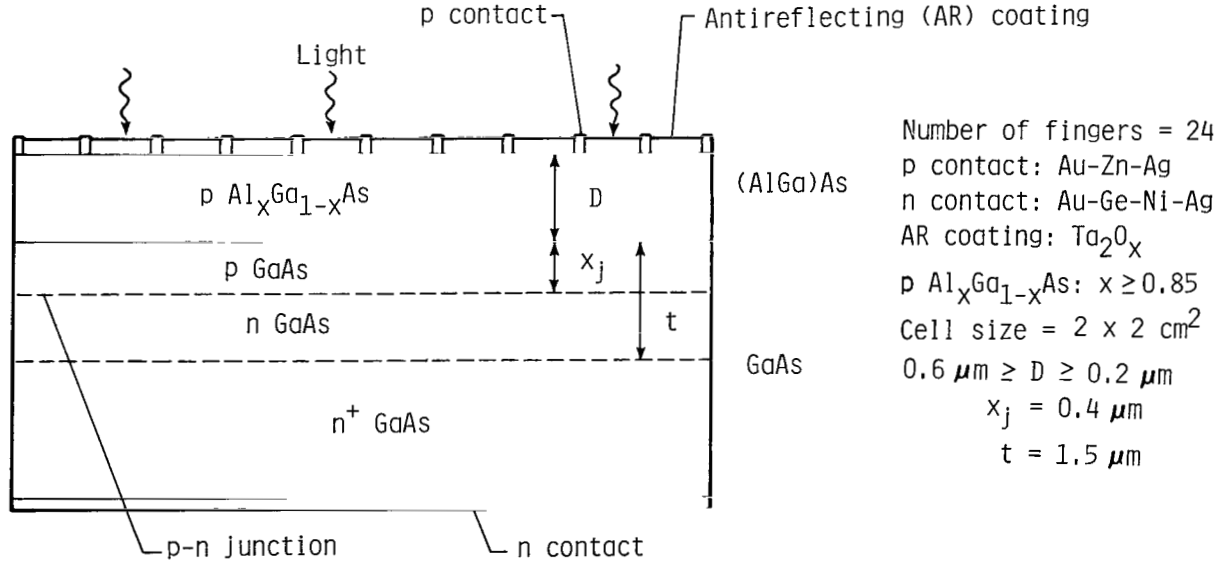

Figure 6.- GaAs solar-cell structure used in present model.

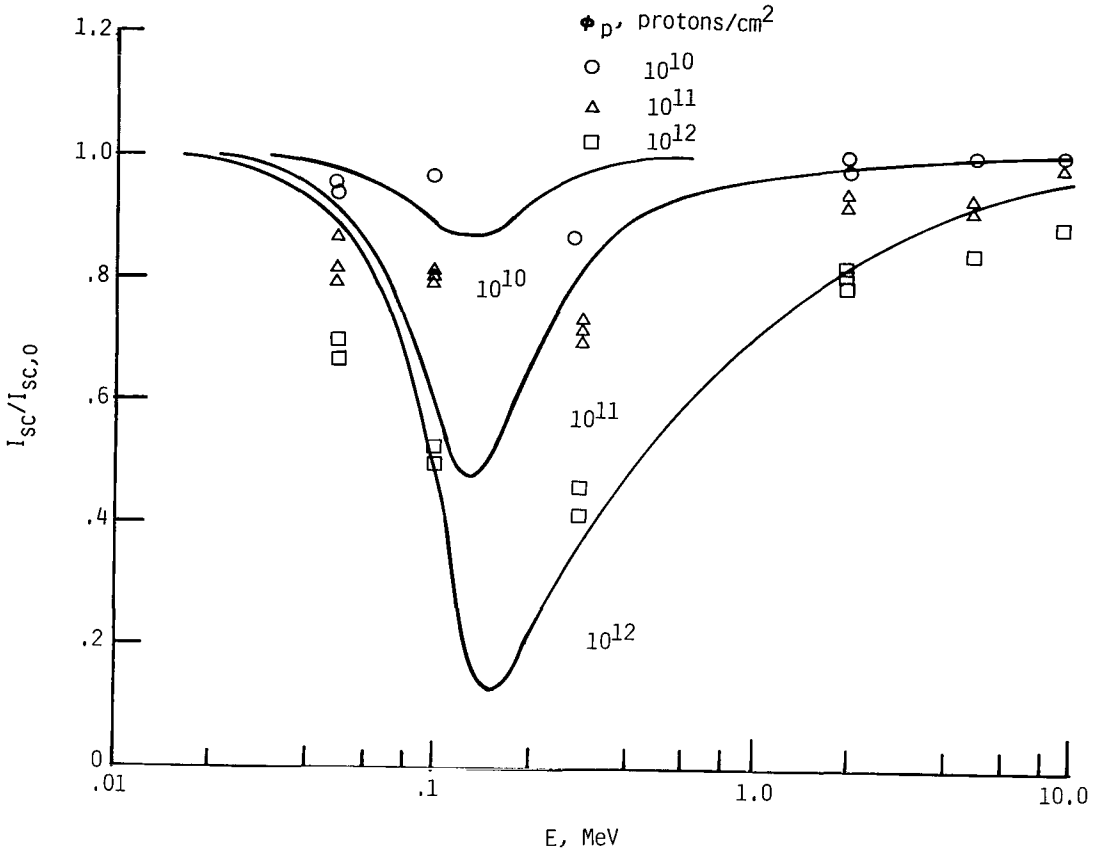

Figure 7.- Reduced short-circuit current for monoenergetic proton exposure at three fluence levels.

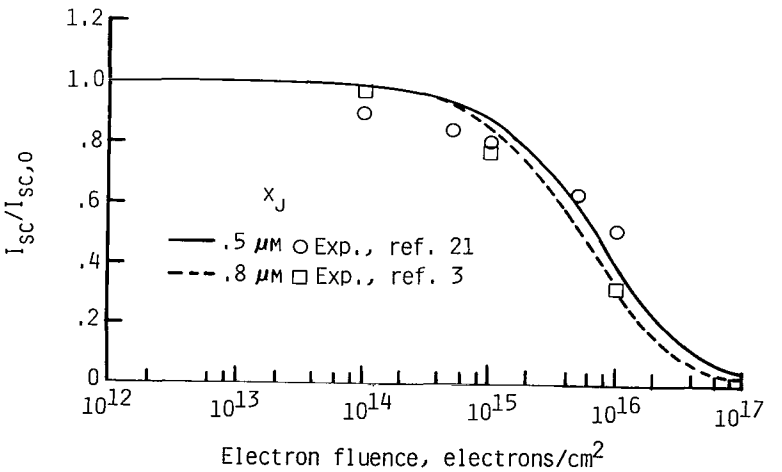

Figure 8.- Reduced short-circuit current after 1 MeV of electron exposure for two junction depths.

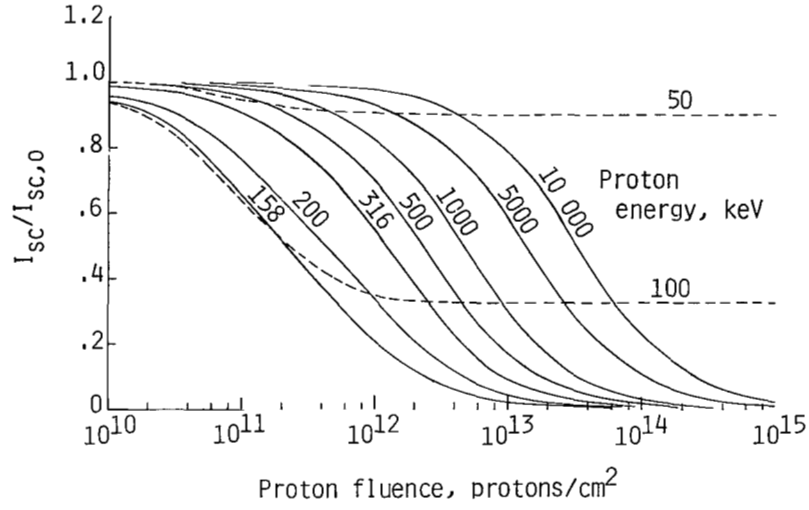

Figure 9.- Reduced short-circuit current for monoenergetic proton exposure for 0.5-μm junction cells.

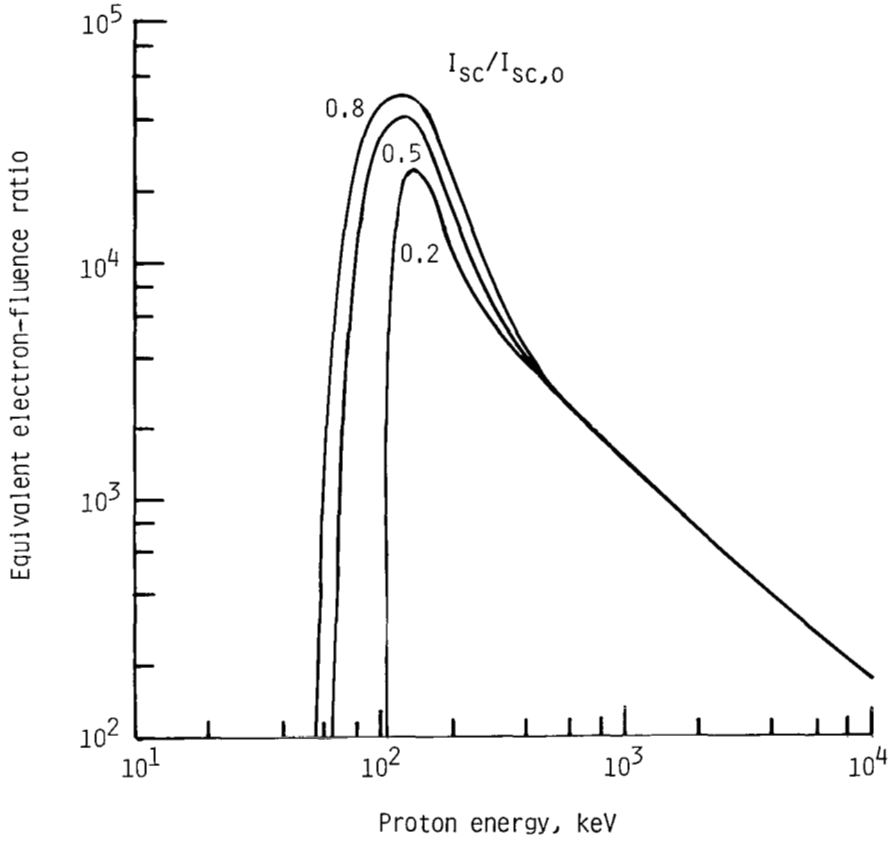

Figure 10.- Equivalent electron-fluence ratio for a cell with 0.5-μm junction depth with a 0.4-μm $Al_xGa_{1-x}As$ window.

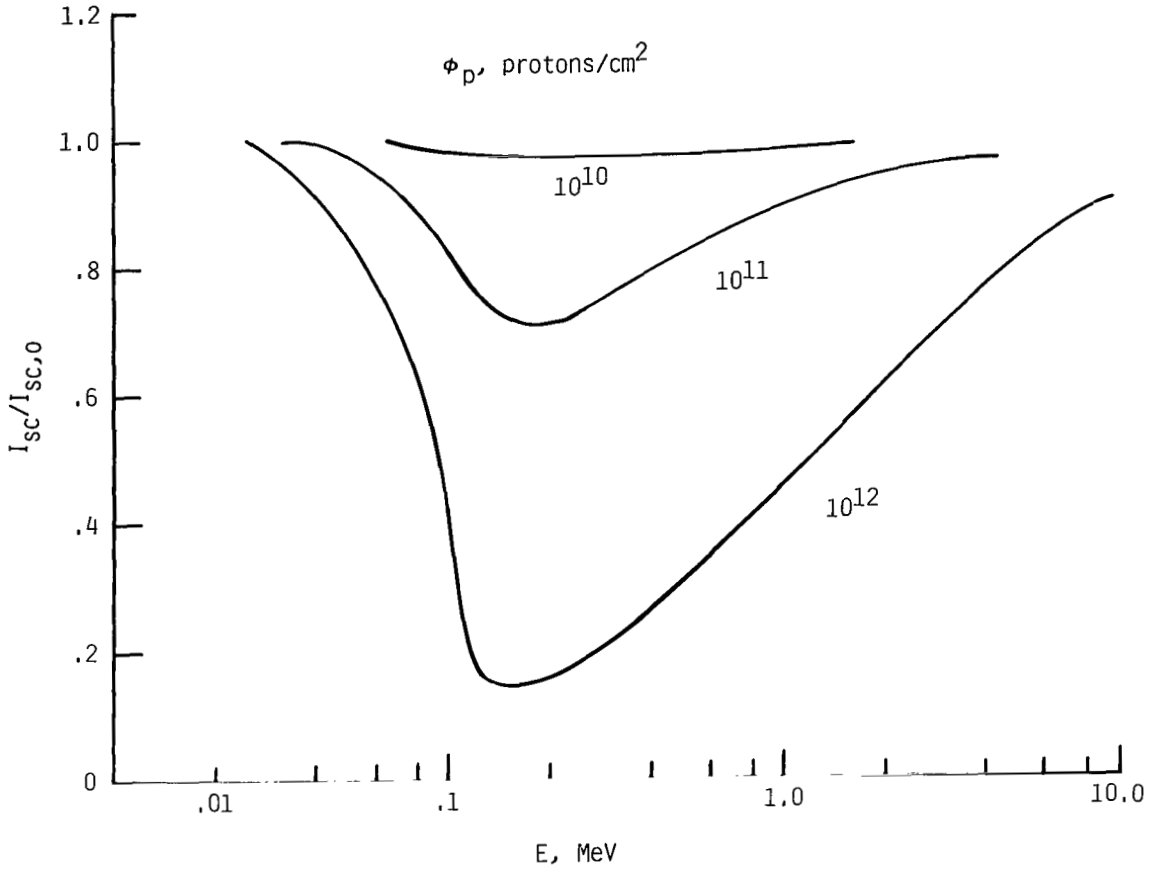

Figure 11.- Reduced short-circuit current for isotropic incident protons at three fluence levels.

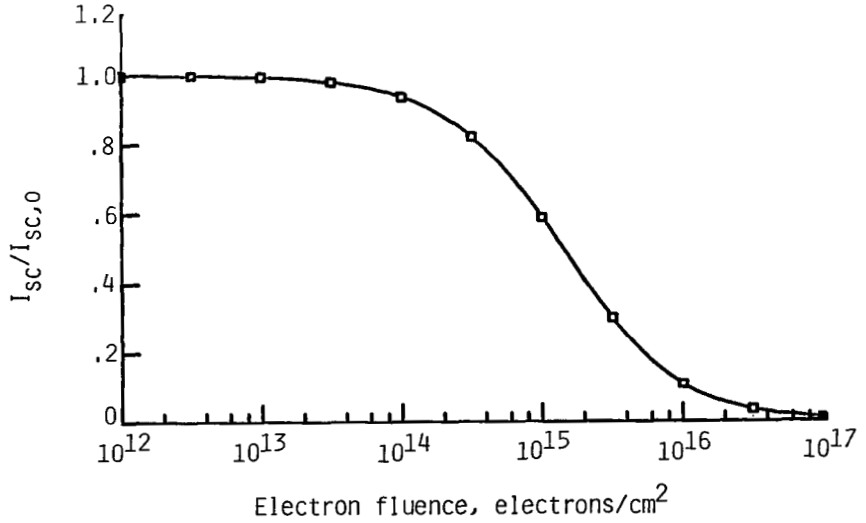

Figure 12.- Reduced short-circuit current for isotropically incident 1-MeV electrons as a function of omnidirectional fluence.

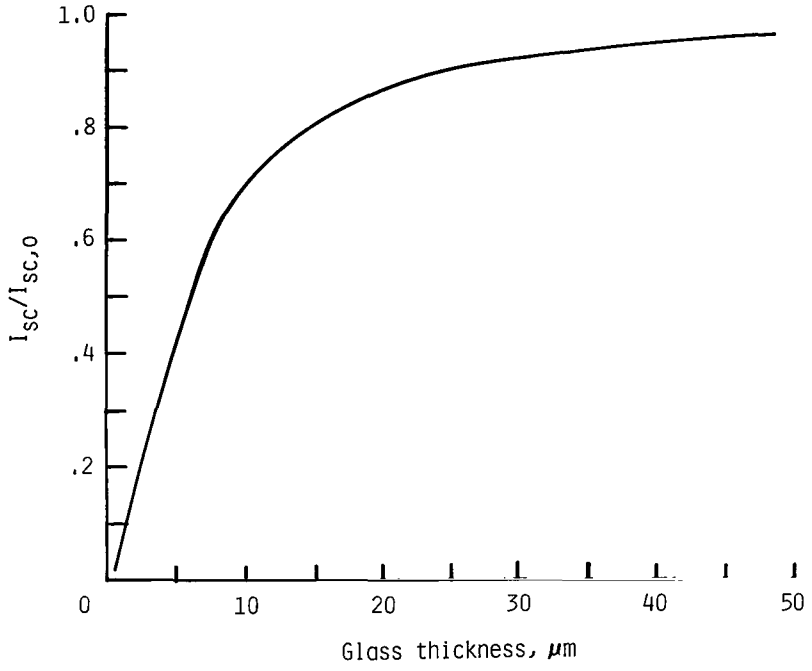

Figure 13.- Reduced short-circuit current due to a large solar event of a cell with a 0.5-μm junction depth with a 0.5-μm $Al_{1-x}Ga_xAs$ window as a function of cover-glass thickness.

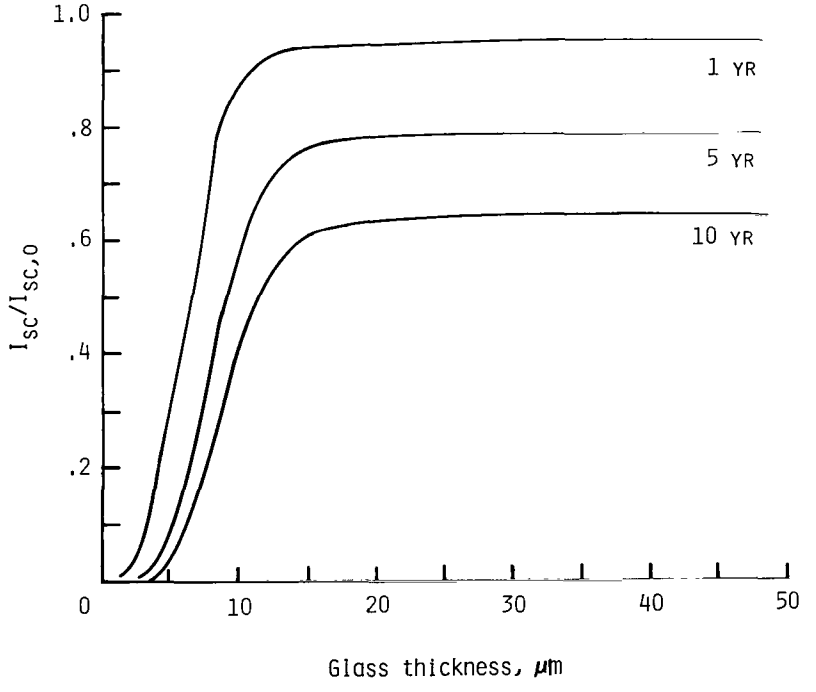

Figure 14.- Reduced short-circuit current of a cell with 0.5-μm junction depth with a 0.5-μm $Al_{1-x}Ga_xAs$ window as a function of cover-glass thickness in geosynchronous environment.

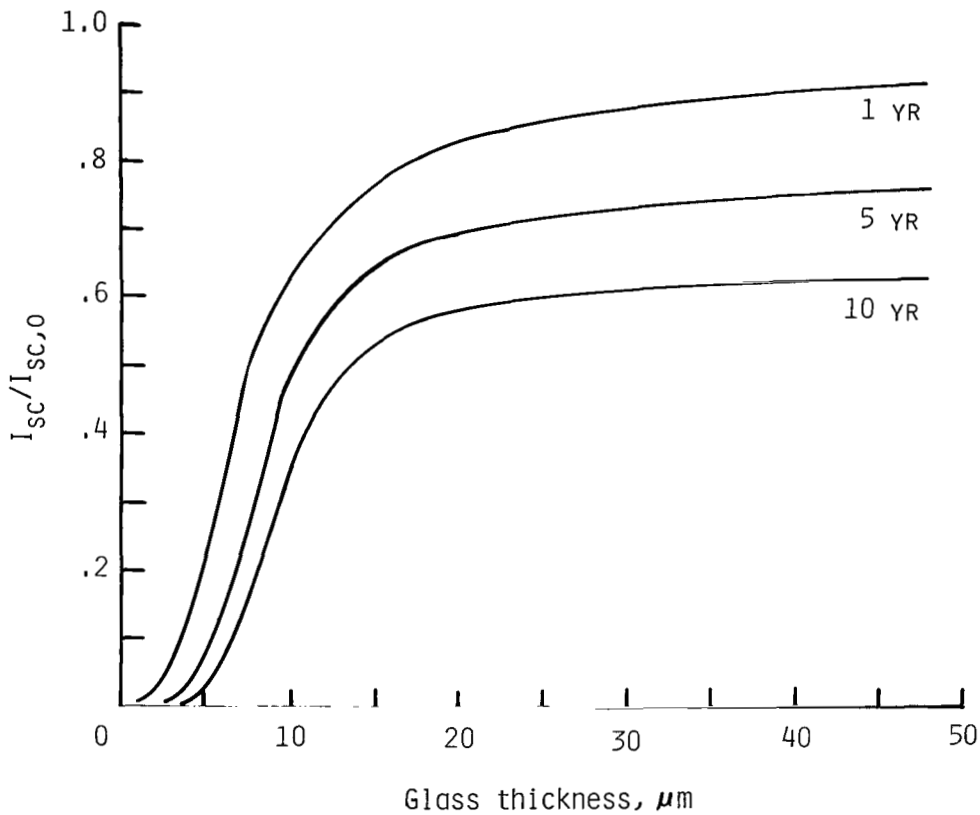

Figure 15.- Reduced short-circuit current of a cell with a 0.5-μm junction depth with a 0.5-μm $Al_{1-x}Ga_xAs$ window as a function of cover-glass thickness in combined geosynchronous and solar cosmic-ray environment.

1. Report No.	2. Government Accession No.	3. Recipient's Catalog No.
NASA TP-2242		

4. Title and Subtitle	5. Report Date
A SIMPLE MODEL OF SPACE RADIATION DAMAGE IN GaAs SOLAR CELLS	December 1983
	6. Performing Organization Code 506-55-43-01

7. Author(s)	8. Performing Organization Report No.
John W. Wilson, John J. Stith, and L. V. Stock	L-15689
	10. Work Unit No.

9. Performing Organization Name and Address	11. Contract or Grant No.
NASA Langley Research Center Hampton, VA 23665	
	13. Type of Report and Period Covered Technical Paper

12. Sponsoring Agency Name and Address	14. Sponsoring Agency Code
National Aeronautics and Space Administration Washington, DC 20546	

15. Supplementary Notes

John W. Wilson: Langley Research Center, Hampton, Virginia.
John J. Stith: Virginia State University, Petersburg, Virginia.
L. V. Stock: Old Dominion University, Norfolk, Virginia.

16. Abstract

A simple model is derived for the radiation damage of shallow-junction gallium arsenide (GaAs) solar cells. Reasonable agreement is found between the model and specific experimental studies of radiation effects with electron and proton beams. In particular, the extreme sensitivity of the cell to protons stopping near the cell junction is predicted by the model. The equivalent-fluence concept is of questionable validity for monoenergetic proton beams. Angular factors are quite important in establishing the cell sensitivity to incident particle types and energies. A fluence of isotropic-incidence 1-MeV electrons (assuming infinite backing) is equivalent to four times the fluence of normal-incidence 1-MeV electrons. Spectral factors common to the space radiations are considered, and cover-glass thickness required to minimize the initial damage for a typical cell configuration is calculated. Rough equivalence between the geosynchronous environment and an equivalent 1-MeV electron fluence (normal incidence) is established.

17. Key Words (Suggested by Author(s))	18. Distribution Statement
Radiation damage Solar cells Semiconductors	Unclassified - Unlimited Subject Category 73

19. Security Classif. (of this report)	20. Security Classif. (of this page)	21. No. of Pages	22. Price
Unclassified	Unclassified	30	A03

For sale by the National Technical Information Service, Springfield, Virginia 22161

NASA-Langley, 1983

National Aeronautics and
Space Administration

Washington, D.C.
20546

Official Business
Penalty for Private Use, $300

THIRD-CLASS BULK RATE

Postage and Fees Paid
National Aeronautics and
Space Administration
NASA-451

3 1U,A, 331219 S00903DS
DEPT OF THE AIR FORCE
AF WEAPONS LABORATORY
ATTN: TECHNICAL LIBRARY (SUL)
KIRTLAND AFB NM 87117

NASA

POSTMASTER: If Undeliverable (Section 158 Postal Manual) Do Not Return